Insights into microtubule catastrophes: the effect of end-binding proteins and force

Kalisch, S.M.J.

The effect of force and end-binding proteins on microtubule catastrophes

5

The dynamics of microtubules are crucial for their biological function. In chapters 3-4 we showed that microtubules are regulated by the end-binding proteins mal3, tea2 and tip1, as well as by forces generated when microtubules grow against cellular obstacles. However, it is unclear whether end-binding proteins qualitatively or quantitatively change the way microtubules respond to force. We therefore investigate microtubules, *in vitro*, in the presence of the end-binding protein complex mal3, tea2, tip1. Head-on forces are achieved by growing the microtubules against micro-fabricated barriers. Using total internal reflection fluorescence microscopy we show that catastrophes occur 5-10 times more frequently in the presence of the protein complex (or mal3 alone) than in its absence. In addition, the distribution of catastrophe times for stalled MTs is strongly peaked for pure tubulin, whereas it is exponentially distributed in the presence of end-binding proteins.

5.1 Introduction

The assembly of tubulin subunits into a microtubule (MT) provides energy [Hill, 1987]. When MTs polymerise against cellular objects they can therefore exert pushing forces [Hotani and Miyamoto, 1990, Fygenson et al., 1997, Inoue and Salmon, 1995, Janson et al., 2003]. This has been demonstrated, for example, on the nuclear positioning in *S.pombe* cells by MTs pushing against both cell ends [Tran et al., 2001]. On the other hand, the microtubule (MT) can generate pulling forces [Mitchison, 1988, Lombillo et al., 1995, Grishchuk et al., 2005] which has been shown during spindle positioning in mitosis [McIntosh and Pfarr, 1991, Barton and Goldstein, 1996, Tran et al., 1997]. That forces are not only used for directly organising the cell interior but also as a regulatory effect was evident from several experiments. *In vitro* MT growth against micro-fabricated barriers reduced the growth speed and increased the catastrophe frequency [Dogterom and Yurke, 1997, Janson et al., 2003, Janson and Dogterom, 2004]. Later, Tischer et al. [Tischer et al., 2009] examined the spatial dependence of MT dynamics in fission yeast cells. The authors provided evidence that MT growth speed and catastrophe time are reduced by compressive forces at the cell pole.
Still, however, little is known about the combined effect of end-binding proteins and forces. To shed light on this we use an *in vitro* assay where MTs grow against

glass barriers generating compressive forces. The MT growth buffer can be completed with the end-binding protein mal3 alone or with the combination of mal3, tea2 and tip1.

5.2 Results

We have shown in chapter 4 that we see catastrophe as a two-step process. In combination with our results from chapter 3, where we determined the disappearance of the EB-binding region as a prerequisite for catastrophe, we conclude that catastrophe is composed of a slow step followed or accompanied by a second short-term step. In chapter 3 we also examined the mal3 attachment to MTs under force and learned that mal3 unbinds when the MT encounters a barrier. What does that mean for the catastrophe process? Janson et al. [Janson and Dogterom, 2004] saw that the catastrophe time distribution for force-loaded MTs in the presence of tubulin is peaked hinting at the mechanism being altered. Whether this is the same in the presence of EBs is a question we want to address in this chapter.

We tackle this problem with an assay very similar to the one described in the previous chapters: From surface-attached stabilised seeds dynamic MTs were nucleated in three conditions: in the presence of
· tubulin
· tubulin and mal3 or
· tubulin and the three EBs, mal3, tea2 and tip1 (referred to as as "mal3-tea2-tip1")
As shown in figure 3.1a-b. the microtubule seeds were, occasionally, positioned such that a dynamic MT could reach the micro-fabricated rigid barriers where they experienced compressive forces. Since only some of the MTs grew against the barriers we could compare the dynamic instability parameters of free MTs to MTs under force. (For the effect of end-binding proteins on free MTs refer to chapter 4).

5.2.1 MTs under force

In figure 3.2 and section 3.2.1 we introduced the types of barrier interactions. We observed two types: "stalling MTs" and "sliding MTs". To decrease the influence of growth speed on catastrophes we only looked at stalling MTs. Furthermore, we are interested in MTs under high load which is the case with stalling MTs. Yet, since the exact magnitude of force was unknown we could only estimate it by plotting MT length when reaching the barrier. As shown in fig. 5.1 all MTs are in the same range of distance to the barrier and thus experience forces of like magnitude. MTs in the presence of tubulin grew slower and switched to shrinkage before they reached too distant barriers (5 μm away). MTs in the presence of mal3 or mal3-tea2-tip1 grew longer and therefore reached barriers further than 6 μm away.

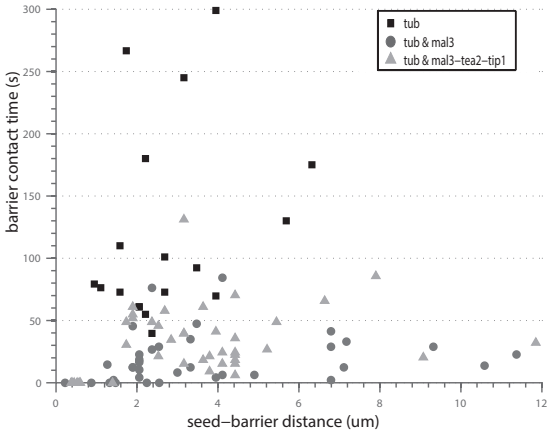

Figure 5.1: Seed-barrier distance for stalling MTs. The length of a stalling, non-buckling dynamic MT indicates the exerted force. The shorter the MT, the higher the force, since longer MTs can release force by buckling [Gittes et al., 1996].

5.2.2 Catastrophe time distributions for MTs under force

For each MT that stalled at the barrier we created kymographs (space-time plots) from the recorded time-lapse TIRF images (see fig. 3.1d-f). In these kymographs we tracked the MT end by hand, where we assigned a straight line to a continuous growth or shrinkage phase, as shown in figure 3.2a. MTs stalling at the barrier contained a free growth part and a barrier-contact part. To avoid confusion we refer to the catastrophe time for MTs under force as "barrier-contact time". We define this as the time spanned from establishment of barrier contact until catastrophe (see white vertical line in figure 3.2a.).

We plot the barrier-contact times as cumulative distribution functions (cdf) (see fig. 5.2) which does not involve binning and therefore shows every measurement. In general, the cumulative distribution at time t indicates the probability of transition to catastrophe in the time span $0-t$. To determine the mechanism of MT catastrophes under force we fitted the experimental data with two distributions, see also figure 4.5 and pages 41ff.:

- The gamma distribution represents multi-step reactions and has been used to describe MT catastrophes [Rice, 1995, Floyd et al., 2010, Gardner et al., 2011b]. It represents a process with multiple steps n where each step happens with an equal characteristic rate $k = \tau^{-1}$. Its cumulative distribution function (cdf) displays a lag phase at the origin.
- The exponential distribution describes a first-order processes implying that catastrophe does not depend on the MT's history. The exponential distribution describes the catastrophe of an intact MT with rate k. The exponential is a special case of a gamma distribution with one step. Exponential cdfs are characterised by a linear slope at the origin.

Looking at figure 5.2 it is clear that the exponential distribution does not fit the tubulin data well. Considering especially the offset at the short times we can discard the barrier contact times to be composed of one step, as shown previously [Janson et al., 2003]. This suggests that multiple steps are necessary until catastrophe. Indeed, a fit with a gamma function reveals approximately three necessary steps

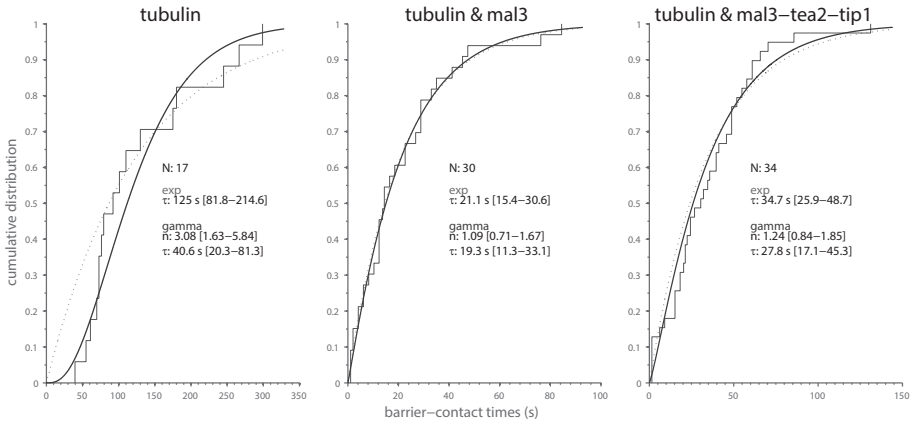

Figure 5.2: Histograms of barrier-contact times and fit results. Barrier-contact times are fitted with an exponential (dotted line) and a gamma distribution (continuous line). Fit results are displayed in the figure with 95% confidence intervals in square brackets. In the presence of EBs, some MTs underwent a catastrophe in between reaching the barrier and recording of the next frame. We assigned here, as an example, to those events a barrier-contact time of 1/2 the average time-lapse interval.

until catastrophe with a time per step of ~40 s. For comparison, when fitting catastrophe times of free MTs with a truncated gamma distribution (see chapter 4) we only found 1.7±0.3 steps, but a time scale of 169±35 s (with 95% confidence intervals). Nevertheless, to be certain about the exact number of steps and the exact timescale for catastrophes under force we would need better statistics. Therefore our main conclusion should be that a catastrophe at the barrier is a process involving several intermediate steps and that this process is faster than the catastrophe process of free MTs.

Free MTs in the presence of end-binding proteins (EBs) transition significantly faster to a shortening state as published previously [Munteanu, 2008, Vitre et al., 2008, Maurer et al., 2011] and shown in section 4.2.3. This raises the question: how do EBs change the catastrophe mechanism of MTs under force? We therefore repeated the experiments with dynamic MTs under force, now in the presence of the end-binding proteins mal3, tea2, tip1 or in the presence of mal3 alone.
In the presence of EBs MTs occasionally underwent a catastrophe when reaching the barrier (referred to as "immediate" events). In these cases it was experimentally hard to determine whether the MT touched the barrier or not. The reason is that TIRF microscopy is not very reliable in terms of absolute flourescent intensity due to reflections at the barrier. Consequently, we could not clearly determine the bulk-barrier interface (±1 pixel). This improved when a MT stalled or repeatedly underwent a catastrophe at the barrier. To determine which of these MTs are unjustly considered to touch the barrier we calculated the catastrophe probability of each of these MTs. We first assumed that these MTs are free. Considering

model	parameter	tubulin	tubulin & mal3	tubulin & mal3-tea2-tip1
exp	τ_{lb}	/	21.0 [15.3-30.5]	34.5 [25.8-48.5]
	τ_{ub}	/	21.2 [15.5-30.7]	34.8 [26.1-49]
gamma	n_{lb}	3.08 [1.63-5.84]	0.88 [0.58-1.34]	0.89 [0.61-1.32]
	n_{ub}	3.08 [1.63-5.84]	1.21 [0.79-1.87]	1.5 [1-2.24]
	τ_{lb}	40.6 [20.3-81.3]	23.9 [13.7-41.6]	38.6 [23.2-64.2]
	τ_{ub}	40.6 [20.3-81.3]	17.5 [10.3-29.7]	23.3 [14.4-37.5]

Table 5.1: Effect of EBs on the catastrophe process. When MTs underwent a catastrophe after reaching the barrier and before the next image was recorded we did not know the exact barrier-contact time. In this case we could only give an upper bound (average framerate) and lower bound (1/10 of the average framerate). We then fitted the barrier-contact times with exponential and gamma distributions. Here we show the fit parameters where $_{lb}$ refers to lower and $_{ub}$ to upper bound and the 95% confidence interval in square brackets. (The results of fitting catastrophe times of free MTs are presented on page 47).

only their age we then calculated the catastrophe probability in the interval [MT age ± the time the MT needs to grow one pixel]. For this we used the truncated gamma distribution and the corresponding parameter estimates determined for free MTs (see p. 47). It turns out that the probability for catastrophe is so small that essentially all the events are considered to happen at the barrier.
Overall, we only observe stalling and sliding MTs at the barrier. However, if a MT undergoes a catastrophe as soon as it reaches the barrier we do not know whether we should count it into the stalling or sliding group. It would be wrong to consider all these "immediate" catastrophe events a priori as stalling. We therefore calculated the fraction of "real" stalling versus "real" sliding MTs and then added the same fraction of immediate catastrophe events to the stalling group.
Having settled on the total number of stalling MTs we still do not know the barrier-contact times of the short events. Similarly to the case of free MTs it is experimentally hard to correctly detect the short events. Since we do not know exactly the barrier-contact time we can only determine an upper (the average framerate) and lower bound where the latter should tend towards zero and was set for computational reasons to 1/10 of the average framerate. Figure 5.2 (middle and right) shows the cumulative distribution plot of barrier-events where the immediate events are set to half the average framerate, as an example. In contrast to the fit for pure tubulin, these fits display a linear slope for very short times and thus are characteristic for a first-order process. Indeed, the gamma function reveals a single step until catastrophe with an approximately 3-times shorter time scale than for free MTs.

We did not fit the barrier-contact times with other distributions since the number of events is too low to allow for interpretation from different models. On the other hand, we consider it very likely that other distributions will also suggest (approximately) one step for the process. The physical interpretations would in

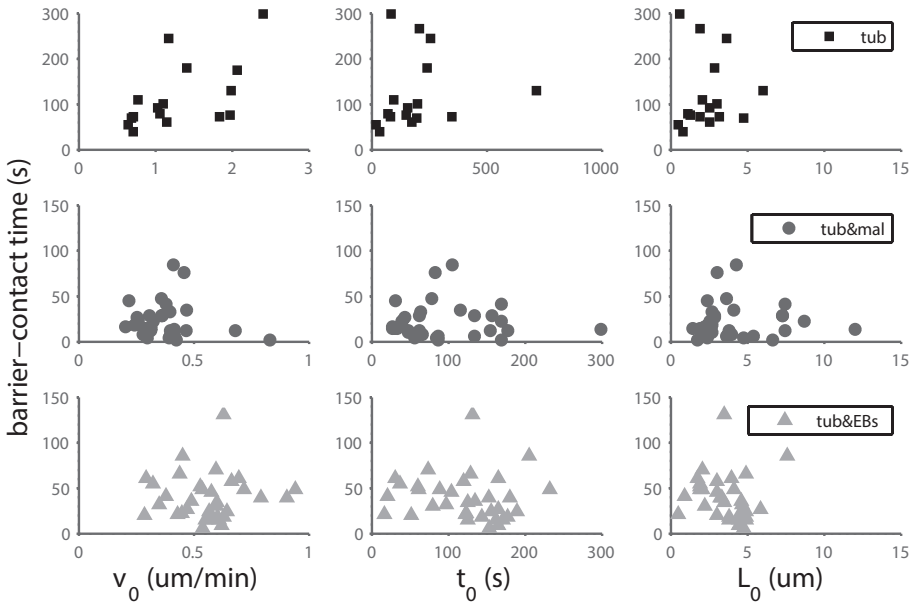

Figure 5.3: Dependence of barrier-contact times on MT parameters before reaching the barrier. Each point represents an individual stalling event for the three experimental conditions of pure tubulin (upper row), tubulin & mal3 (middle row) and tubulin & mal3-tea2-tip1 (lower row). **left column.** Barrier-contact times are plotted versus growth speed v_0 at which MT approached the barrier, **middle column.** versus MT "age" t_0 and **right column.** MT length L_0 when reaching the barrier.

this case be the same.

We showed in chapter 4 that the catastrophe time of free MTs is dependent on their growth time (their age). In our analysis of barrier-contact times we did not take into account the time the MT was growing freely. Contrary, we considered the MT upon reaching the barrier to have no age. That is because we think that the free catastrophes and barrier-contact times could be seen as two independent processes. Indeed, the time until catastrophe at the barrier is much shorter than for free MTs making the former the dominant step. Therefore, we assume not to have a big influence of MT age on barrier-contact times. Further, a plot of MT growth time vs. barrier-contact time did not show a correlation, see figure 5.3. Neither did we recognise an influence of MT length or pre-barrier growth speed on barrier-contact times, as shown previously [Janson and Dogterom, 2004].

5.3 Discussion

Our data provides insight into the events leading to a transition of MTs under force from growth and stalling to a shortening state. By TIRF microscopy we determined the duration MTs spend in contact with a barrier. To get a better insight into the catastrophe process we fitted our data with exponential and gamma distributions. MTs grown in the presence of tubulin alone evolved in at least two independent steps before the onset of shrinking. This is not unexpected: the same peaked distribution after reaching the barrier has been shown before [Janson and Dogterom, 2004]. Janson et al. [Janson, 2002, Janson et al., 2003] showed that catastrophe time depends on the tubulin on-rate which can be decreased by both force and tubulin concentration. We can thus assume that also here the force decreases the growth speed of MTs under force. Specifically, we do not have a good explanation for he strongly peaked distribution of catastrophe times at this moment. To understand how force affects the catastrophe process of MTs grown from pure tubulin further experiments are hence necessary.

In the presence of a force and of mal3 or mal3-tea2-tip1, both the exponential and the gamma distribution fit well, where the latter suggests 0.8-1.5 necessary steps until catastrophe (error margin as we cannot precisely determine the catastrophe time of the very short events, see above). This makes catastrophe under force in the presence of EBs effectively a Poissonian process. Our findings of free MTs in the presence of EBs show that catastrophe happens in two steps with a step of ~60 s followed up or accompanied by a shorter step of ~15 s or 20-30 s, respectively (see section 4.2.4). We reasoned that the shorter step must be defined by the random occurrence of the tubulin transformational change. As presented in figure 4.10 on page 53 this change comprises the nucleotide change from the EB1-competent state into the for mal3 unfavoured GDP-state. The duration of this step agrees very well with the time scale obtained from the fit of barrier-contact times. Therefore, we believe that the single step under force in the presence of EBs also comprehends the nucleotide transformation. Consequently, the first step, observed only for free MTs, must be so much shortened under force and with EBs that it appears to happen immediately. In the case of free MTs, the accomplishment of the first step puts MTs into a state where they could catastrophe after one more (the second random) destabilizing event. The omission of this first step in the case of force-loaded MTs renders them directly after barrier contact "ready" for catastrophe.

Previous publications reported that catastrophe occurred more often at the cell periphery than in the cytoplasm [Komarova et al., 2002, Brunner and Nurse, 2000b, Drummond and Cross, 2000, Tran et al., 2001]. More specifically, the mal3 and tip1 RNAis by Brunner and Busch [Brunner and Nurse, 2000b, Busch and Brunner, 2004] might suggest that tip1 protects against the small forces at the cell periphery (not at the cell ends). Yet, this does not agree with our data. Within errorbars it seems rather that tip1 gives a slight protection against catastrophes both on free and loaded MTs. The difference between *in vitro* and *in vivo* results most probably stems from other, yet presently unknown, binding partners of EB1

in vivo [Komarova et al., 2009].

5.4 Methods

Sample preparation. Barriers made of SiO (glass) were micro-fabricated on glass cover slips as described in chapter 2.2.1. Afterwards the cover slips were rinsed with iso-propanol and then rinsed 3x with MilliQ. A flowchamber was assembled by parallelly gluing two strips of parafilm between a microscope slide and a coverslip (Merck, Darmstadt, Germany). The flow chamber was functionalised and passivated with a 0.2 mg/ml mix of biotin-PLL-PEG and PLL-PEG (SurfaceSolutions, Switzerland). Residual non-specific binding sites were blocked with 0.5 mg/ml κ-casein and 1 % F-127. Stabilised, fluorescently labelled MT seeds (containing 12 % fluorescent tubulin and 18 % biotin tubulin) were attached by means of a biotin-streptavidin linker. Microtubule growth was initiated by adding MRB80 buffer (80 mM K-PIPES pH 6.8, 50 mM KCl, 4 mM $MgCl_2$, 1 mM GTP, 1 mM EGTA, 10 mM 2-mercaptoethanol), 0.5 mg/ml κ-casein, an oxygen scavenger system (20 mM glucose, 200 μg/ml glucose-oxidase, 400 ug/ml catalase), 15 μM tubulin of which 5-7 % was labelled with rhodamine, HiLyte488 or HiLyte647 (Cytoskeleton, Denver, CO, USA). Optionally, end-binding proteins (EBs) were added: either 200 nM mal3-Alexa488 alone or together with 8 nM tea2 and 50 nM tip1 (in the latter case also 2 mM ATP was added to the MRB80 buffer). EBs were purified as described in [Bieling et al., 2007]. Unless stated otherwise, chemical reagents were obtained from Sigma-Aldrich (Saint-Louis, MO, USA).

Imaging method. The sample was imaged in an inverted Ti-Nikon Eclipse microscope (Nikon, Tokyo, Japan) using total internal reflection fluorescence (TIRF) microscopy equipped with a 1.49 NA, 100x oil immersion objective. Single tiff-images were recorded using a Calypso 491 nm diode laser (Cobolt, Solna, Sweden), a Jive 561 nm diode laser (Cobolt) and a 635 nm "56 RCS-004" diode laser (Melles Griot, Albuquerque, NM, USA) imaged with a Roper Scientific Coolsnap HQ CCD-camera (Photometrics, Tucson, AZ, USA) and saved to disk with MetaMorph software (Molecular Devices, Sunnyvale, CA, USA), at time-lapse intervals between 0.2 and 5 s, at typical exposure times of 200-250 ms. After mounting the sample on the microscope stage imaging started after a 5 minute equilibration time. Imaging time was kept below 2 hours (average of 1 hour) at a constant temperature of $25 \pm 0.5°C$ which was maintained by running heated/cooled water through a sleeve around the objective. Simultaneously, the water temperature was adjusted by Peltier elements to a temperature based on a sensor within the sleeve in proximity to the sample.

Data analysis. Tiff-stacks were background-subtracted and bleach-corrected (macro developed by J. Rietdorf, EMBL Heidelberg, Germany) in Fiji (based on ImageJ which was developed by Wayne Rasband, NIH in Bethesda, MD, USA). Growth trajectories of single MTs were displayed in kymographs where straight lines were fitted to each growth or shrinkage phase by hand/mouse. A phase was defined as continuous growth or shrinkage at constant speed. We define the barrier-contact time as the time spanned from reaching the barrier until catastrophe. Coordinates of the line fits were processed in Matlab (Mathworks, Natick, NA, USA) by a custom-made software to determine dynamic instability parameters per sample.

Fitting. All unbinned data was pooled together for each experimental condition and was used for distribution fitting. The distribution parameters were estimated and the corres-

ponding confidence intervals given by using the maximum likelihood statistics toolbox of Matlab. The exponential distribution was fitted using the *expfit* function and for the gamma distribution we used the *gamfit* function.

Acknowledgements

We are grateful for the help and advice with the micro-fabrication received from Chris Rétif and Hans Zeilemaker. Further, we thank Peter Bieling and Thomas Surrey for help with the protein purification of mal3, tea2 and tip1. We highly appreciate the help of Roland Dries with the imaging. The work presented in this chapter was carried out as part of the EU Program AMOCROSS, as part of a "VICI" grant provided by the "Nederlandse Organisatie voor Wetenschappelijk Onderzoek (NWO)" and as part of the research program of the "Stichting voor Fundamenteel Onderzoek der Materie (FOM)", which is financially supported by the "Nederlandse Organisatie voor Wetenschappelijk Onderzoek (NWO).